Biodiesel Spray Characteristics and Their Effect on Engine Combustion and Particulate Emissions

Article · March 2023

DOI: 10.1115/1.4045923]

CITATIONS
0

READS
103

2 authors:

Akhilendra Pratap Singh
Indian Institute of Technology Kanpur
102 PUBLICATIONS **3,619** CITATIONS

SEE PROFILE

Avinash Kumar Agarwal
Indian Institute of Technology Kanpur
582 PUBLICATIONS **23,245** CITATIONS

SEE PROFILE

Biodiesel Spray Characteristics and Their Effect on Engine Combustion and Particulate Emissions

Akhilendra Pratap Singh
Engine Research Laboratory,
Department of Mechanical Engineering,
Indian Institute of Technology Kanpur,
Kanpur 208016, Uttar Pradesh, India

Avinash Kumar Agarwal[1]
Engine Research Laboratory,
Department of Mechanical Engineering,
Indian Institute of Technology Kanpur,
Kanpur 208016, Uttar Pradesh, India
e-mail: akag@iitk.ac.in

Spray analysis is used to characterize the fuel spray evolution and spray shape, which affects in-cylinder combustion and particulate emission characteristics of compression ignition (CI) engines. In this study, spray evolution of biodiesel blends and mineral diesel was captured using a high-speed charge coupled device (CCD) camera at different fuel injection pressures (FIPs) and ambient pressures (APs) in a constant volume spray chamber (CVSC). Results showed that spray parameters were significantly affected by FIP and AP. Higher FIPs resulted in longer fuel spray penetration length (L_s) and reduced spray cone angle (A_s). However, AP variation showed an exactly opposite trend of L_s and A_s. Increasing AP resulted in shorter L_s and increased A_s. Fuel properties also affected the spray characteristics, which slightly improved for lower biodiesel blends (B20: 20% v/v blend of biodiesel with mineral diesel) and then degraded for higher biodiesel blends (B40: 40% v/v blend of biodiesel with mineral diesel) with respect to baseline mineral diesel. The effects of these findings of fuel spray analysis were validated using engine experiments, which were performed in a single-cylinder research engine using identical test fuels and fuel injection parameters. Relatively superior combustion of B20-fueled engine and lower particulate emissions at higher FIPs showed good agreement with spray results. [DOI: 10.1115/1.4045923]

Keywords: spray characteristics, fuel atomization, biodiesel, spray evolution, combustion, particulates, renewable energy

1 Introduction

The homogeneity in fuel–air mixture in the engine cylinder directly affects combustion, performance, and emission characteristics of diesel engines [1,2]. For diesel engines, it is desirable that fuel spray jet should enter the combustion chamber with high velocity and fuel spray should atomize into fine droplets. Smaller fuel droplets enable rapid vaporization of fuel, promoting fuel–air mixing [3]. Therefore, it becomes necessary to study spray characteristics such as spray evolution, spray breakup, and fuel atomization in the engine combustion chamber. However, this is very challenging due to intense and continuously changing in-cylinder conditions. For such investigations, the availability of optical access is the most critical requirement. Therefore, many researchers performed experiments in a constant volume spray chamber (CVSC), where actual engine combustion chamber conditions were created, except temperature and turbulence. Such experiments are termed as "cold chamber experiments," and spray investigations are performed in the absence of combustion. Visualization of spray in the CVSC shows the liquid fuel distribution, which provides useful information about spray evolution and macroscopic spray parameters such as spray penetration length (L_s), spray cone angle (θ_s), and spray area (A_s). These macroscopic spray parameters are determined by using segmentation processing of the images captured by high-speed CCD camera. L_s represents the longitudinal limit of fuel spray droplet distribution inside the combustion chamber, which can be measured as the distance between the tip of the injector nozzle to the farthest point, where the spray diminishes. θ_s represents the width of the spray, which is defined as the angle created by the tip of the injector nozzle and tangents drawn on the spray boundary. A_s is defined as the area covered by fuel spray droplets within the spray regime, which can be calculated as the sum total of the image pixels captured by the CCD camera [3,4].

In CVSC experiments, fuel is injected in the pressurized chamber through an injector nozzle at constant fuel injection pressure (FIP). The ambient pressure (AP) inside the CVSC can be taken as the in-cylinder pressure at the time of fuel injection for better accuracy of the results. Both parameters, FIP and AP, are important for diesel engines, which should be optimized according to engine operating conditions [5]. Several researchers carried out spray investigations in the CVSC to assess the effect of FIP and AP on macroscopic spray characteristics. Roy [6] reported that the combination of optimized start of injection (SoI) timing and FIP resulted in less odorous emissions from diesel engines. Li et al. [7] performed spray experiments using blends of oxygenated additives with mineral diesel at different FIPs and reported that L_s increased with increasing FIP. They also investigated the effect of AP on fuel's macroscopic spray characteristics. It was found that increasing AP of CVSC reduced L_s; however, spray plume became wider compared with lower AP conditions. At higher AP, increased ambient air density played an important role and enhanced ambient resistance, which reduced the axial momentum of the fuel spray. Mohan et al. [8] reported that θ_s was not affected significantly by FIP; however, AP variations showed a significant effect on θ_s. Agarwal et al. [9] also reported that increasing FIP was beneficial for spray optimization and resulted in lower emissions compared with engines operating at lower FIPs. Variations in AP became more critical for advanced combustion techniques, where fuel was injected very early (in presence of low in-cylinder temperature and pressure conditions) in the compression stroke for improving the fuel–air mixing. Agarwal et al. [10] critically reviewed the spray characteristics of common rail direct injection (CRDI) diesel engines and reported that FIP and SoI timings should be optimized according

[1]Corresponding author.
Contributed by the Internal Combustion Engine Division of ASME for publication in the Journal of Energy Resources Technology. Manuscript received May 30, 2019; final manuscript received December 27, 2019; published online January 10, 2020. Assoc. Editor: Hameed Metghalchi.

to engine operating conditions, in order to avoid fuel spray impingement on the cylinder walls and also to enhance fuel–air mixing.

In the last few decades, researchers have also focused on the development of technologies for the utilization of alternative fuels such as biodiesel, alcohols, etc. in diesel engines. Among different alternative fuels, oxygenated fuels are preferred due to their higher fuel oxygen content, which reduces particulate formation during combustion [11–13]. However, these alternative fuels have different properties such as density, kinematic viscosity, volatility, surface tension, boiling temperature, etc. which also play an important role in spray formation, spray evolution, and spray atomization [4,14–16]. Hence, it becomes necessary to explore the effects of these alternative fuels on the spray characteristics. Kegl and Lesnik [17] compared the macroscopic spray characteristics of biodiesel and mineral diesel, and they reported that biodiesel had a longer L_s compared with baseline mineral diesel. Yu et al. [18] also performed spray experiments using biodiesel and baseline mineral diesel and the results showed relatively lower θ_s and A_s for biodiesel compared with baseline mineral diesel. These studies suggested that biodiesel has relatively inferior spray atomization characteristics compared with baseline mineral diesel, which adversely affects fuel–air mixing, leading to inferior engine performance and emission characteristics. Therefore, researchers suggested that if mineral diesel is to be replaced by biodiesel, then it becomes essential to optimize the fuel injection parameters according to the properties of new test fuel [5,19–22]. Tat and Van Gerpen [19] reported that the use of biofuels in diesel engines require advanced fuel injection timing due to relatively higher bulk modulus of ethyl and methyl esters of soy oil compared with baseline mineral diesel. Sayin et al. [20] also reported that methyl esters required advanced fuel injection timings for reducing hydrocarbon (HC), carbon monoxide, and particulate emissions. Few researchers suggested that biodiesel spray characteristics can be improved by using second-generation biodiesel [23]. Pachiannan et al. [24] reported that hydrogenated catalytic biodiesel showed relatively shorter spray liquid length compared with mineral diesel, which resulted in relatively superior fuel atomization and reduced possibility of spray wall impingement.

Most studies in the open literature focused either on fuel spray characterization or on the engine combustion and emission characteristics. Very few studies are available, which validated the findings of spray investigations through the combustion and emission results of engine experiments. In this study, spray investigations have been carried out in a CVSC using three test fuels, namely, B20 (20% v/v blend of biodiesel with mineral diesel) and B40 (40% v/v blend of biodiesel with mineral diesel) and baseline mineral diesel at different FIPs (400, 700, and 100 bars) and APs (10, 20 and 30 bars). Spray evolution images were captured by a high-speed CCD camera and images were analyzed for understanding spray evolution and calculation of macroscopic spray parameters, namely, spray penetration length (L_s), spray cone angle (θ_s), and spray area (A_s). The findings of these spray investigations were validated through engine experiments using similar FIPs and ambient conditions. Engine experiments were performed in a single cylinder research engine fueled by all three test fuels. Fuel injection parameters such as FIP and SoI timings were selected according to the in-cylinder conditions of the spray experiments, in order to minimize the experimental errors. Results of spray experiments were compared with the in-cylinder combustion and particulate emission characteristics of the test engine, which were expected to be significantly affected by fuel's spray characteristics in a diesel engine. A qualitative correlation between the fuel's spray parameters and engine's combustion and emission characteristics remain a novel and innovative aspect of this study.

2 Experimental Setup and Methodology

For this study, an experimental setup was designed to investigate the spray characteristics in a cold, non-reacting environment of a CVSC. In this setup, spray experiments were performed under similar conditions as that of the engine combustion chamber, but without the turbulence and heat release conditions. This experimental setup consisted of four sub-systems, namely, CVSC, fuel injection system, chamber pressurization system, and image acquisition system. The schematic of the experimental setup is given in Fig. 1.

To investigate the spray characteristics, a cubical shaped constant volume spray visualization chamber (CVSC) was designed at the Engine Research Laboratory, IIT Kanpur [25]. This cubical spray chamber had four side flanges for optical access (for illuminating the chamber using an intense, flicker-free white light source and for capturing spray evolution images using a high-speed CCD camera), one flange at the top (for mounting the solenoid fuel injector) and one flange at the bottom (for N_2 inlet, N_2 outlet, and for mounting a pressure gauge). The chamber was pressurized by using nitrogen gas and the chamber pressure was controlled by a pressure regulator, which was fitted on to the nitrogen bottle connected to the spray chamber. A pneumatic high-pressure fuel pump (Maximator; G300 LVE) was used for supplying the fuel to the solenoid injector (Bosch; CP3 VCO) through a common rail. This pneumatic pump works on the principle of "pressure intensifier." The outlet pressure was calculated by the transmission ratio between an air piston and plunger, multiplied by the drive ratio. A custom-built injector driver (NI; 780718-01) was used to control the injection parameters of the peak and hold type solenoid injector. The injector driver system had a reverse polarity circuit, integrated controller and chassis (NI; CompactRIO-9022), direct injector driver modules (Drivven; D000020), and digital input module (NI; NI-9411). Triggering of fuel injector was synchronized with the CCD camera in order to eliminate the delay between the fuel injection and the captured images.

A high-speed CCD camera (Photron; Fastcam 675K-C1) was used to capture the spray images. Two mirror stands were fabricated and used, which provided the desired view for capturing the spray evolution images. To illuminate the spray in the CVSC, a flicker-free white light source (NaBa Green; 24W) was used. This white light source was capable of producing high-intensity light (36,078 lux, 10 cm from the source and 1523 lux, 50 cm from the source). Captured images were processed using a MATLAB code, in which the original spray image was transformed into a binary image, wherein the pixel representation for the background (dark region) was "0," while the pixel representation for spray (bright region) was "1." The intensity of the image was varied using the Gaussian threshold factor multiplied to the original spray image, which provided the boundary of the spray. After imposing the injector tip details in the binary image, various macroscopic spray parameters were calculated. For validation of spray results, engine experiments were carried out in a single-cylinder diesel engine. This engine was equipped with a common rail direct injection (CRDI) system, which injected fuel upto 1600 bar FIP. Fuel injection parameters of this engine were controlled by an electronic control unit (ETAS; ETK 7.1), through which, upto four injections could be done in a single-engine cycle. Other details of the test engine could be seen in our previous publications [26,27]. For combustion analysis, a dedicated high-speed data acquisition (DAQ) system (AVL; Indimicro) was used, which acquires data from the piezoelectric pressure transducer (Kistler; 6013) synchronised with the angle encoder (AVL; 365). This DAQ system was capable of acquiring, storing, and analyzing the combustion data simultaneously [26]. Particulates emitted in the engine exhaust were measured using an engine exhaust particle sizer (TSI; EEPS 3090), which was capable of measuring particles in the size range of 5.6 nm to 560 nm. EEPS is suitable for internal combustion (IC) engines because it can measure up to #10^8 particles/cm^3 of the exhaust gas. The working principle and detailed technical specifications of EEPS can be seen in our previous publications [28,29]. Table 1 shows the comparative properties of various test fuels.

Table 1 shows that increasing biodiesel content in the test fuel increased the viscosity and density. These two properties are very important for spray characteristics [19,20].

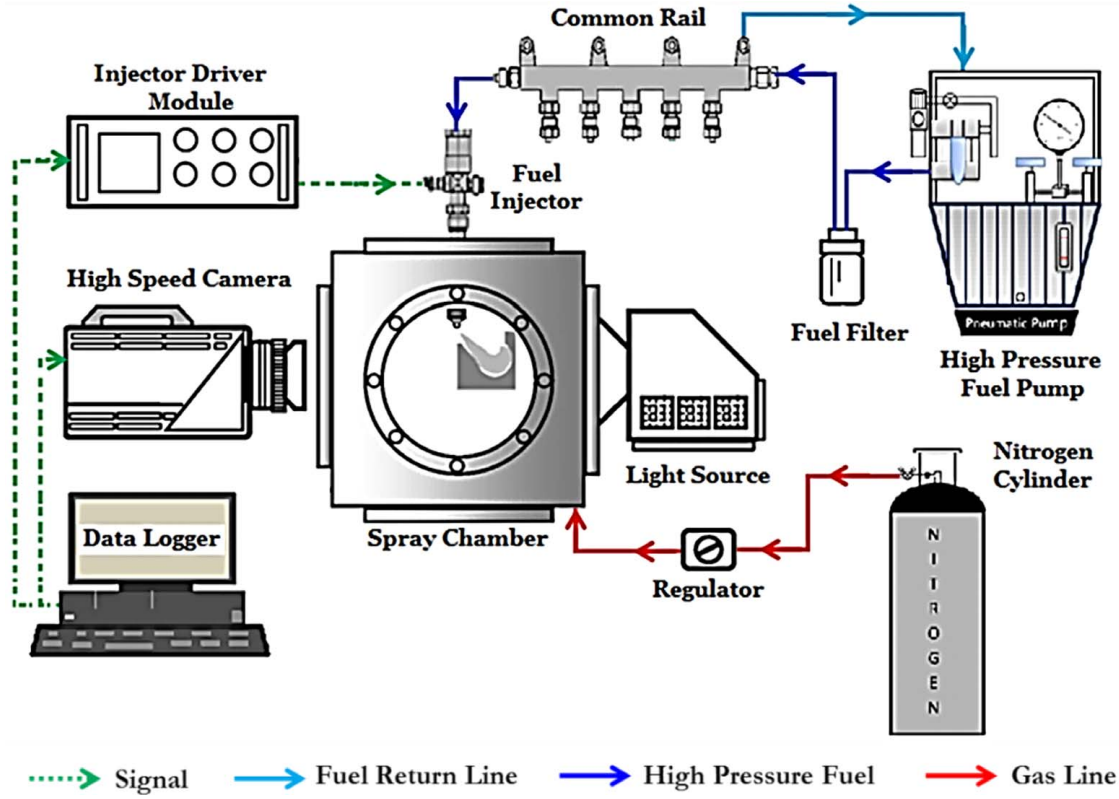

Fig. 1 Schematic of the experimental setup for spray characterization

3 Results and Discussion

Results of this experimental study are divided into five subsections, namely, effect of FIP on spray development, effect of AP on spray development, effect of fuel composition on spray development, comparison of macroscopic spray parameters of different fuels at different FIPs and APs, and experimental validation of the spray results using engine experiments. To investigate the effects of FIP and AP, spray experiments were performed using mineral diesel only; however, all three test fuels were used for investigating the effect of fuel properties.

3.1 Effect of Fuel Injection Pressure. Figure 2 shows the spray images of mineral diesel captured by a high speed camera (frame rate = 10,000 fps) at three different FIPs (400, 700, and 1000 bars). During this experiment, AP was kept constant at 20 bar. All experiments were carried out for fixed fuel injection quantity (10 mg/cycle).

Figure 2 shows that higher FIP resulted in a relatively smaller fuel droplet size due to improved fuel atomization, which leads to a quicker evolution of spray structure compared with lower FIPs. At higher FIPs, relatively shorter injection duration for the same

Table 1 Comparison of test fuel properties

Property	Mineral diesel	B20	B40
Composition (v/v)	100% diesel	20% biodiesel and 80% diesel	40% biodiesel and 60% diesel
Calorific value (MJ/kg)	43.54	42.63	41.16
Viscosity (cSt) @ 40 °C	2.82	3.17	3.34
Density (g/cm^3) @ 30 °C	0.831	0.846	0.857
Cetane number	~47	~48	~49
Flash point (°C) (min)	~54	~71	~103

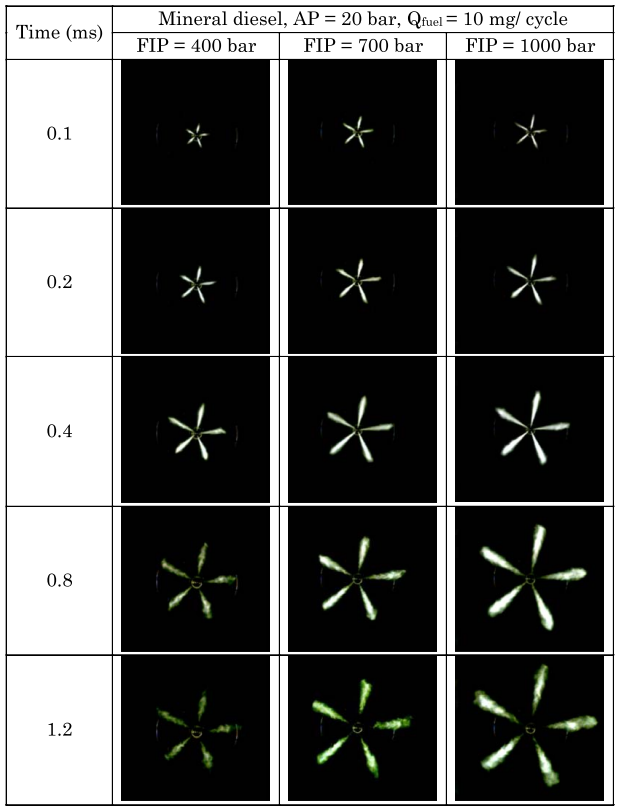

Fig. 2 Effect of FIP on mineral diesel spray evolution at constant AP (20 bar) in the CVSC

fuel injection quantity might be another reason for a quicker evolution of the fuel spray. Shortly after the fuel spray was fully evolved, slight fluctuation in the spray profile was observed (at $t = 1.2$ s) due to breaking of fuel droplet clusters around the periphery of the fuel spray, which was more dominant on the leading edge of the spray tip (Fig. 2). Ejim et al. [30] also reported that increasing FIP improved the evaporation of spray droplets due to smaller Sauter mean diameter (SMD). Figure 2 shows relatively longer L_s at higher FIPs, which was mainly due to higher momentum of fuel spray droplets, which penetrate quickly in the CVSC. Higher FIPs resulted in a higher velocity of liquid fuel in the injector orifice, leading to improved fuel atomization at the exit from the nozzle. Higher cavitation might be another important reason for longer L_s at higher FIPs. Cavitation happens due to fluid acceleration, directional changes in the fluid flow and pressure difference between the FIP and AP. Increasing FIP results in relatively longer L_s due to collapse of these cavitation bubbles in the nozzle orifice, leading to severe perturbations downstream. Figure 2 shows that the tendency of cavitation diminishes with reducing FIP and consequently L_s decreases as well. At 400 bar FIP, cavitation occurs in a very small region, therefore the effect of cavitation is not significant, which leads to shorter L_s at lower FIP. For diesel engines, higher L_s is desirable for improving the fuel–air mixing, which results in superior combustion and lower particulate emissions. However, too high FIP leads to spray impingement at the piston bowl lip and the cylinder liner, which in-turn deteriorates the engine performance, resulting in higher HC emissions. Therefore, the selection of suitable FIP for diesel engines is essential for satisfactory engine performance and emissions characteristics. Figure 2 shows that the spray plumes become narrower at higher FIPs, i.e., smaller θ_s. Reduction in θ_s was mainly due to quicker fuel atomization and greater vaporization compared with lower FIPs.

3.2 Effect of Ambient Pressure. Figure 3 shows the spray images of mineral diesel captured by high-speed CCD camera (frame rate = 10,000 fps) at different APs (10, 20, and 30 bars). APs were selected on the basis of in-cylinder pressures at different SoI timings (pilot and main) in motoring conditions. During the experiment, FIP was kept constant at 700 bar. All experiments were carried out for fixed fuel injection quantity (10 mg/cycle).

Figure 3 shows that L_s was dominantly affected by the AP. At low AP (10 bar), L_s was long enough for spray impingement at piston bowl lip and cylinder liner, which was highly undesirable. Increasing AP resulted in shorter L_s due to increased ambient air density, which offered greater resistance to the spray leaving the injector nozzle. This resulted in slower spray evolution and reduced axial momentum of spray droplets, leading to relatively shorter L_s at the same time after the start of injection. This could be seen in all spray images at the same time frame, especially at $t = 0.1$ ms, where spray plumes were not visible at AP = 30 bar. Higher air resistance caused faster dispersion of spray plumes and prevented them from reaching their maximum tip penetration point, which resulted in shorter L_s. Figure 3 showed that θ_s became larger with increasing AP. The resistance offered by dense air was the main reason for this behavior. Overall, this experiment showed that the spray evolution was superior at higher AP, which promoted quicker dispersion of fuel spray droplets. This finding emphasized on suitable fuel injection timing of diesel engines to improve fuel–air mixing for better engine performance and lower emissions. This can also be related to the engines running at higher compression ratios, where fuel is directly injected in higher AP environment, leading to higher thermal efficiency.

3.3 Effect of Fuel Composition. Figure 4 shows the spray images of mineral diesel, B20 and B40 captured by high-speed CCD camera (frame rate = 10,000 fps) at constant AP (20 bar) and FIP (700 bar). All experiments were carried out for fixed fuel injection quantity (10 mg/cycle).

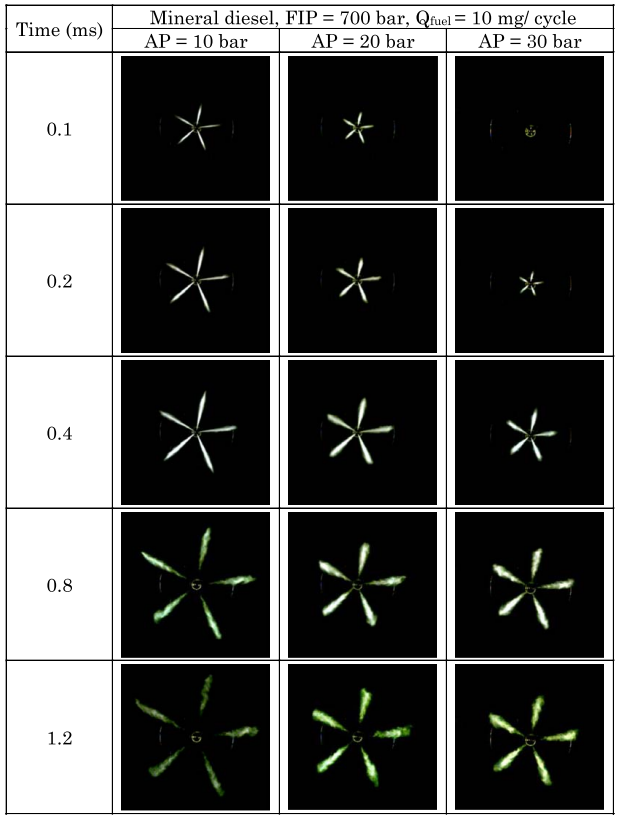

Fig. 3 Effect of AP on mineral diesel spray evolution at constant FIP (700 bar) in the CVSC

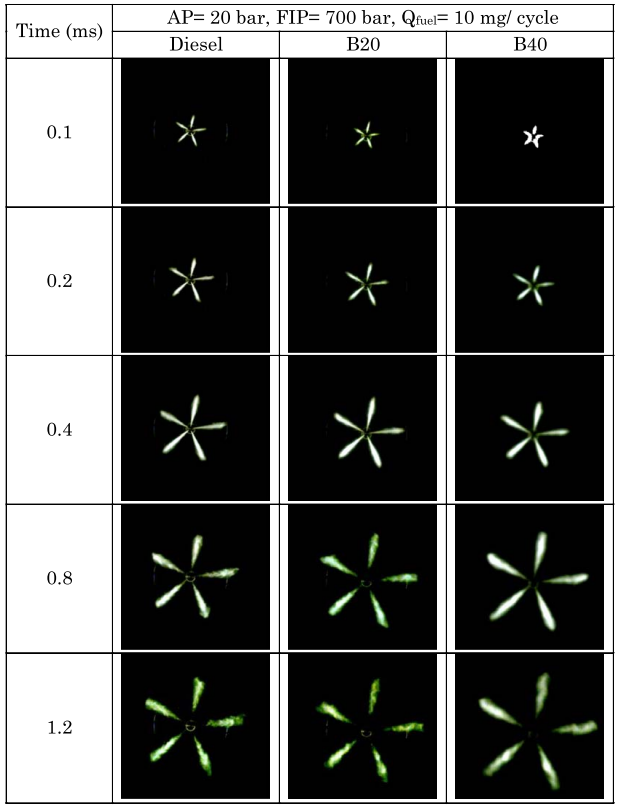

Fig. 4 Comparative spray evolution of mineral diesel, B20 and B40 at constant AP and FIP in the CVSC

Figure 4 shows that fuel properties such as kinematic viscosity, density and surface tension, etc. play an important role in spray evolution and spray atomization. From Fig. 4, it can be seen that atomization of biodiesel blends was relatively inferior compared with baseline mineral diesel. Relatively higher viscosity and surface tension of biodiesel might be a possible reason for this trend, which prevents spray breakup into small droplets. Few researchers suggested that the atomization of biodiesel blends can be improved by increasing the FIP (Fig. 2) [10]. Figure 4 showed that θ_s of mineral diesel was the highest amongst all test fuels, which decreased slightly with increasing biodiesel fraction in the test fuels. It was evident from Fig. 4 that mineral diesel had relatively shorter L_s compared with biodiesel blends.

Spray images showed that fuel with higher biodiesel fraction (B40) exhibited a longer, denser spray core pattern. This was visualized in the spray development as spray images of B40 exhibited relatively more whitish color and longer spray plumes compared with mineral diesel and B20. This might be due to relatively higher viscosity of biodiesel, which resulted in larger SMD of spray droplets compared with lower blends of biodiesel (B20) and baseline mineral diesel [10]. Vortex shape spray of B20 and B40 with higher viscosity was denser compared with mineral diesel, which may be due to lower breakup frequency of viscous fuels. Lower breakup rate of B20 and B40 produced larger size droplets and caused the spray pattern to become denser compared with baseline mineral diesel. Comparison of spray images also revealed that for the same instant after the start of injection, B20 and B40 showed slightly retarded spray evolution compared with mineral diesel. This may be due to delayed response of injector for viscous fuels such as B20 and B40. Patel et al. [3] also reported similar behavior of biodiesel blends.

3.4 Effect of FIP and AP on Spray Parameters. In this section, spray images of mineral diesel, B20 and B40 captured at different FIPs (400, 700, and 1000 bars) and APs (1, 10, 20 and 30 bars) were processed in "MATLAB" for calculating macroscopic spray parameters, namely, spray penetration length (L_s), spray cone angle (θ_s), and spray area (A_s). All experiments were performed thrice and the average of the image post-processing results was presented. Standard procedure was used to calculate the measurement errors/instrument errors which were presented as error bars in the results, in order to take care of experimental uncertainty. For all test fuels, L_s increased with increasing FIP. Increasing AP resulted in shorter L_s due to resistance offered by the high-density ambient air. Since the fuel quantity used for spray atomization was constant (10 mg/cycle), therefore it was obvious that a larger area of spray dispersion resulted in shorter L_s. Figure 5 showed that the spray penetration of mineral diesel was the lowest amongst all test fuels at all APs. This was because of the lowest density and viscosity of mineral diesel amongst the test fuels, which resulted in rapid atomization of mineral diesel compared with other test fuels. Atomization was an important phenomenon in IC engines because it resulted in breakup of bulk liquid jets into smaller droplets. Viscosity also affected spray characteristics because it affected continuous film formation of fuel emerging out from the injector nozzle, followed by ligament and bag formation, before disintegration into individual droplets at the time of spray breakup. Increased viscous forces result in a lower tendency of liquid distortion, which reduces the rate of disruption of the fuel packets into tiny fuel droplets. Finally, this produces longer L_s, which is clearly visible in the results of B20 and B40. Higher fuel density (specific gravity) and surface tension were the two other factors contributing to inferior spray characteristics of biodiesel blends. In general, fuel density affected spray compactness and penetration; however, these effects were not significant in the case of biodiesel blends (Fig. 5).

Spray parameters showed a strong correlation with surface tension. L_s increased with increasing biodiesel fraction in the test fuels, which was due to higher surface tension of B20 and B40. Higher surface tension forces reduced irregularities on the boundary of the spray plume, which prevented the formation of spray ligaments and disintegration of fuel jet into tiny fuel droplets. From Fig. 5, it can be observed that increasing FIP resulted in relatively narrower sprays, which represented smaller θ_s. Increasing AP resulted in larger θ_s compared with lower APs; however, the effect of AP variation was less significant compared with FIP variations. For all test fuels, θ_s increased with increasing AP mainly due to increased ambient air density, which resulted in inhibitive action for spray development [31]. Feng et al. [32] also reported similar

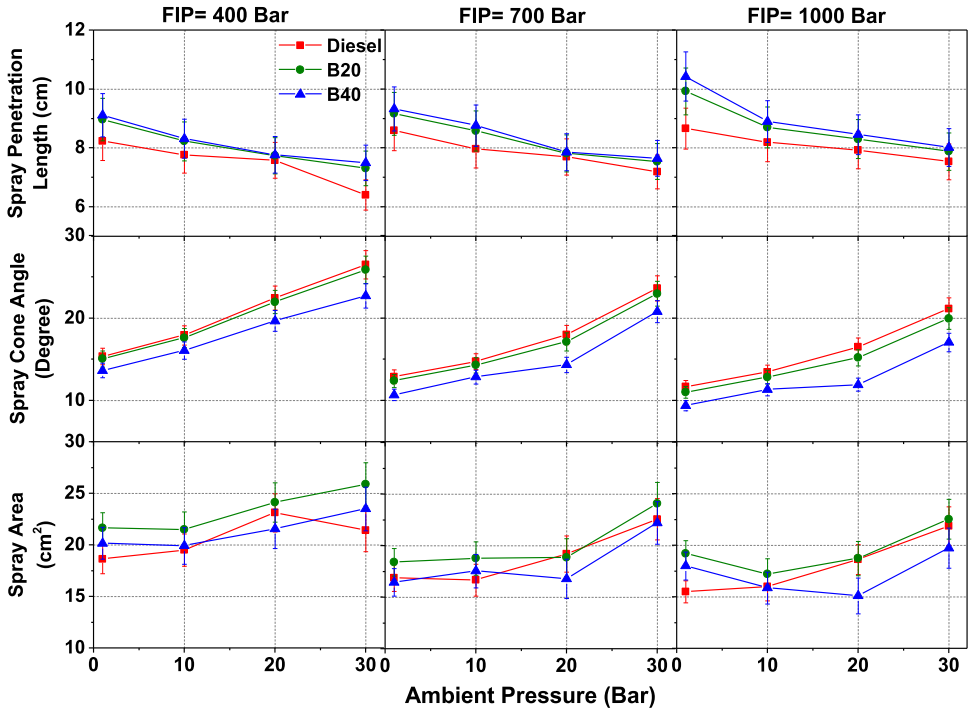

Fig. 5 Macroscopic spray parameters at different FIPs and APs for mineral diesel, B20 and B40

results. Effect of fuel properties was clearly visible on θ_s. Amongst all test fuels, mineral diesel exhibited highest θ_s, which decreased with increasing biodiesel fraction in the test fuels. Guan et al. [33] also observed a similar spray pattern for diesel and biodiesel. During fuel atomization, relatively smaller θ_s for biodiesel blends caused spray impingement into high-temperature regions, where an abundance of oxygen readily oxidized fuel, which resulted in higher NO_x formation.

A_s is another important macroscopic spray parameter, which should be larger for diesel engines because it affects the interaction of fuel spray droplets with the ambient air. Larger A_s is a qualitative measure of fuel–air mixture homogeneity [34]. A_s showed an irregular behavior at different FIPs and APs. This irregular behavior was attributed to relatively greater dominance of L_s and θ_s. At most experimental conditions, B20 showed the maximum A_s, and B40 exhibited the minimum A_s. With increasing FIP, A_s of all test fuels decreased, which showed the dominance of L_s over θ_s. Increasing AP resulted in higher A_s of mineral diesel and B20; however, A_s of B40 increased at 400 bar and then decreased at higher FIPs. Higher AP promoted breakup of fuel droplets into smaller ones, which subsequently produced larger θ_s and spray width but shorter L_s with denser spray.

3.5 Combustion and Particulate Emission Characteristics of Engine for Validation of Spray Results. For validating spray results, a single-cylinder research engine was used for the experiments using mineral diesel, B20 and B40. All engine experiments were carried out at constant engine load (3 bar brake mean effective pressure (BMEP)) and speed (1500 rpm). Experiments were performed at three FIPs (400, 700, and 1000 bars) and three starts of the main injection (SoMI) timings (12 deg, 16 deg, and 20 deg before top dead center (bTDC)). For all experiments, other parameters such as the start of pilot injection (SoPI) timing and exhaust gas recirculation (EGR) were kept constant at 35 deg bTDC and 12%, respectively. These experimental conditions for the engine were exactly the same, at which the spray experiments were conducted in the CVSC. The engine experimental results are divided into two sub-sections, namely: (i) effect of FIP and fuel properties on combustion and particulate emissions (Fig. 6), and (ii) effect of SoMI timing and fuel properties on combustion and particulate emissions (Fig. 7). In the second sub-section, the effect of SoMI timing on combustion and particulate emission characteristics is an attempt to establish a correlation with the spray experiments performed at different APs. At advanced SoMI timings, relatively lower in-cylinder pressures correspond to 10 bar and 20 bar AP; however, SoMI timing near top dead center (TDC) corresponds to ~30 bar AP.

Figures 6(*a*)–6(*c*) show the in-cylinder pressure and heat release rate (HRR) variations with respect to crank angle position at different FIPs using mineral diesel, B20 and B40. Other parameters such as SoMI timing, SoPI timing, and EGR were kept constant at 12 deg bTDC, 35 deg bTDC, and 12%, respectively. Combustion results showed that increasing FIP resulted in improved combustion, which was in line with the results of spray experiments in the CVSC (Fig. 2). At higher FIPs, improved fuel atomization resulted in homogeneous fuel–air mixing, which was clearly visible in the in-cylinder pressure curves, where the peak of in-cylinder pressure curves (P_{max}) increased with increasing FIP [35]. This can also be seen in HRR trends, in which peak HRR increased with increasing

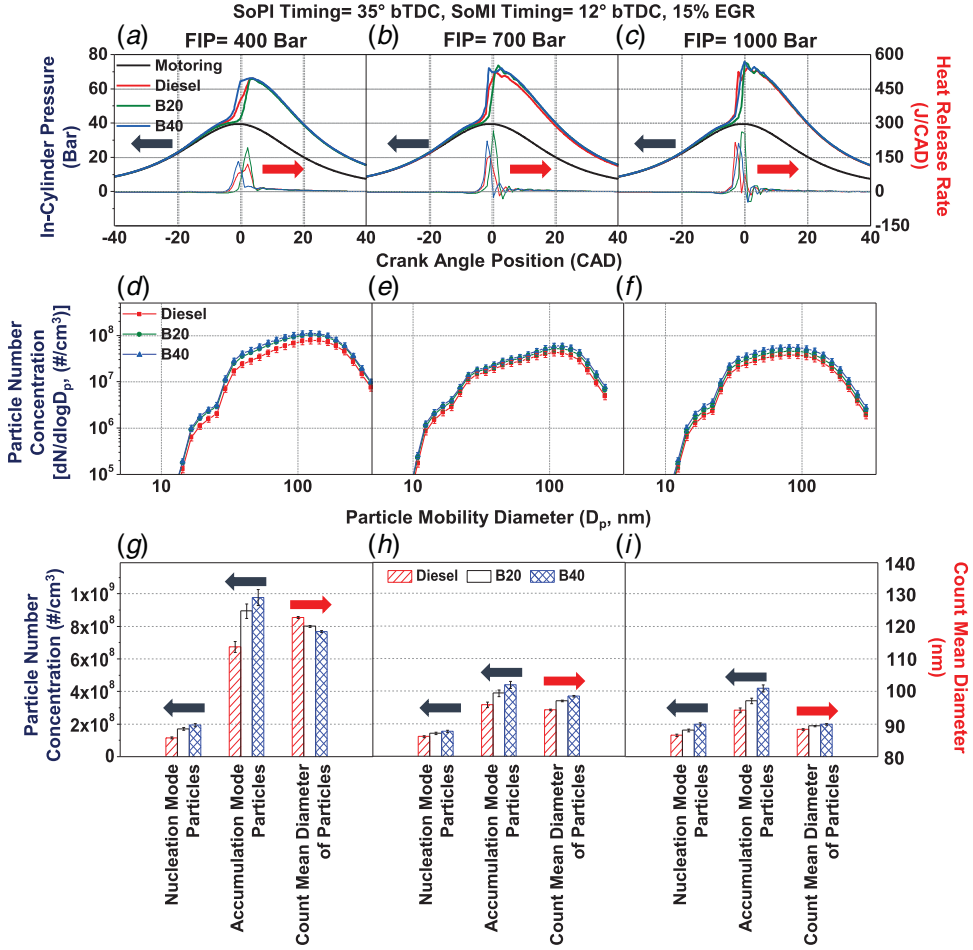

Fig. 6 Combustion and particulate emission characteristics of mineral diesel, B20 and B40 fueled engine at different FIPs

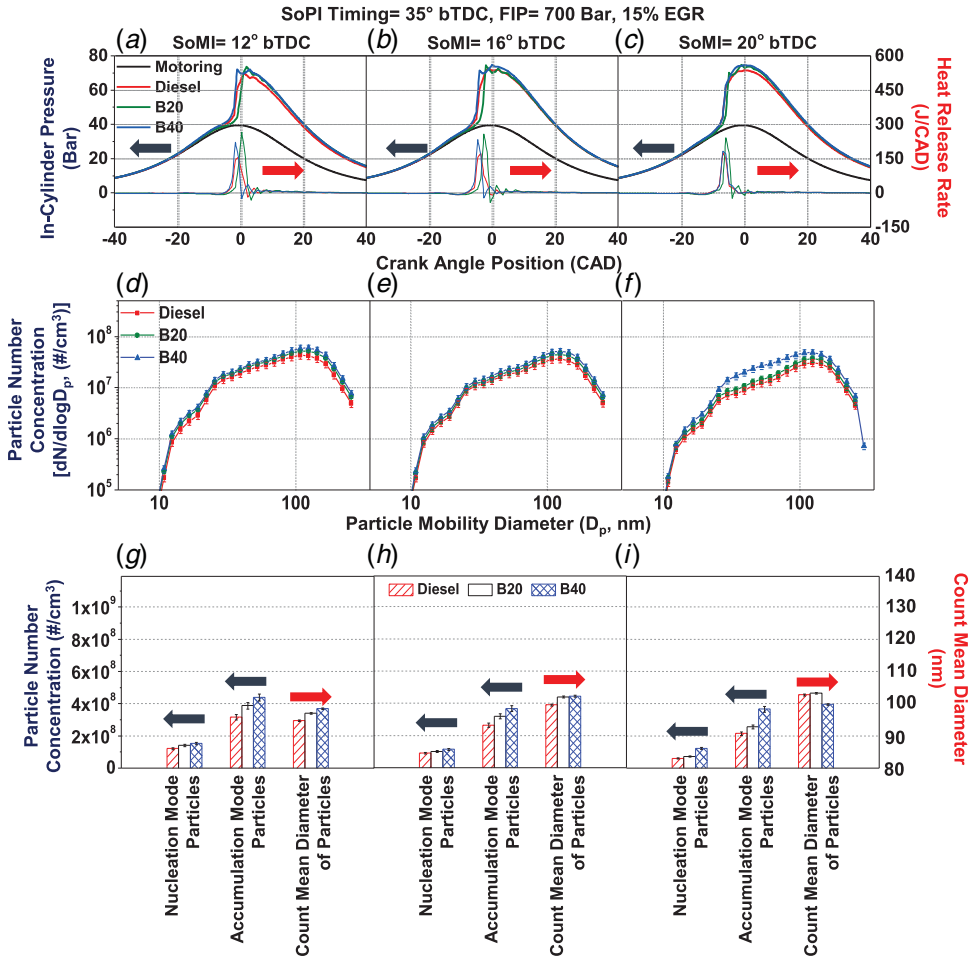

Fig. 7 Combustion and particulate emission characteristics of mineral diesel, B20 and B40 fueled engine at different SoMI timings

FIP. This showed dominance of premixed combustion phase over the diffusion combustion phase due to improved fuel–air mixing. Advancement of combustion events with increasing FIP was another important observation (Figs. 6(*a*)–6(*c*)), which showed a good correlation with the spray results (Fig. 2). At higher FIPs, shorter injection duration due to high velocity of fuel droplets and shorter ignition delay due to improved fuel atomization were the two main reasons for advanced combustion events at higher FIPs. At 1000 bar FIP, knocking was also observed in the in-cylinder pressure curves (Fig. 6(*c*)), which might be due to too short ignition delay and spray impingement on the cylinder walls (Fig. 2).

The effects of fuel properties were also reflected in the engine's combustion characteristics. At lower FIPs, the relative dominance of chemical and physical delay due to physical and chemical properties of test fuels was clearly visible on the combustion characteristics. Physical properties of B20 such as higher viscosity, higher surface tension, and higher diffusion coefficient compared with mineral diesel affected the physical delay due to inferior fuel spray atomization, vaporization, and fuel–air mixing, which resulted in the retarded start of combustion (SoC). However, chemical properties of B40 such as carbon chain length and H/C ratio resulted in faster fuel–air chemical kinetics, leading to slightly advanced SoC. Due to improved fuel spray atomization, the relative dominance of these fuel properties became less effective at higher FIPs, leading to relatively lower difference between SoC (Figs. 6(*b*) and 6(*c*)).

Figures 6(*d*)–6(*i*) show the particulate emission characteristics, namely, particle number-size distribution, number concentration of nucleation mode particles (NMPs), accumulation mode particles (AMPs), and count mean diameter (CMD) of particles emitted from mineral diesel, B20 and B40 fueled engine at different FIPs. Particulate emission results showed that increasing FIP resulted in a lower number concentration of particles emitted. Increasing FIP resulted in improved fuel–air mixing, which prevented formation of fuel-rich zones in the combustion chamber, where soot formation took place. With increasing FIP, shifting of peak of particle number-size distribution curves toward smaller size particles was another important finding, which was closely related to the spray characteristics. Particle number-size distributions showed that engine fueled with biodiesel blends emitted relatively higher number of particles compared with baseline mineral diesel. This observation also validated the finding of spray investigations, which showed relatively inferior spray characteristics of biodiesel blends compared with baseline mineral diesel. With increasing biodiesel fraction in the test fuels, peak of particle number-size distribution shifted toward bigger particles, which indicated relatively bigger nuclei formation from biodiesel combustion. This may also be due to greater agglomeration of particles emitted from biodiesel fueled engines [36]. Figures 6(*g*)–6(*i*) showed that the accumulation mode particles emitted from all test fuels were higher at all FIPs. This is a typical characteristic of diesel engines [37]. With increasing FIP, number concentration of AMPs decreased, however NMPs remained almost the same. At all FIPs, relatively higher number concentration of NMPs and AMPs emitted from biodiesel fueled engine was another important observation, which increased with increasing biodiesel fraction in the test fuels. Variation in CMD of particles showed good agreement with the spray characteristics. For all test fuels, CMD of particles decreased with increasing FIP due to improved fuel

atomization characteristics. At 400 bar FIP, increasing biodiesel fraction in the test fuel resulted in lower CMD of particles, however at higher FIPs, this trend reversed and CMD of particles increased with increasing biodiesel content. This finding exhibited dominance of fuel properties and FIP on particulate emission characteristics, which was also observed in the spray investigations.

Figures 7(*a*)–7(*c*) show the in-cylinder pressure and HRR variations with respect to crank angle position at different SoMI timings using mineral diesel, B20 and B40. Other parameters such as FIP, SoPI timing, and EGR were kept constant at 700 bar, 35 deg bTDC, and 12%, respectively. Results showed that advancing SoMI timing provided greater time for fuel–air mixing, which improved the combustion characteristics and resulted in relatively more stable combustion compared with retarded SoMI timings. At advanced SoMI timing, relatively lower in-cylinder pressure created lower resistance to spray evolution, which can also be seen in spray results in the CVSC (Fig. 3). Effect of advancing SoMI timing was also visible in the HRR trends, where peak HRR slightly decreased with advancing SoMI timings (Figs. 7(*a*)–7(*c*)). This may be due to relatively inferior fuel spray atomization, which resulted in weaker premixed phase combustion compared with retarded SoMI timing. This finding was also in agreement with the CVSC spray results, where lower AP resulted in slightly inferior fuel spray characteristics compared with higher APs (Fig. 3). At all SoMI timings, variations in P_{max} were not significant; however, advanced SoMI timing resulted in more stable combustion. Advanced SoMI timing also resulted in relatively earlier combustion, however the rate of advancement in combustion events was relatively lesser compared with SoMI timing. Relatively lower in-cylinder pressure at the time of advanced SoMI timing was the main reason for this behavior, which resulted in slower combustion event [38,39]. Similar results were also seen in the CVSC spray investigations, where lower AP degraded the spray quality.

Similar to FIP, fuel properties also affected the combustion characteristics at different SoMI timings. However, the relative dominance of chemical and physical properties of test fuels was not as strong as in the effect of FIP variation. At retarded SoMI timings, B20 showed slightly retarded SoC and B40 showed advanced SoC compared with baseline mineral diesel. At advanced SoMI timings, all test fuels showed the same SoC. The availability of more time due to advanced SoMI timing was the main reason for this trend, which dominated over the effect of fuel properties.

Figures 7(*d*)–7(*i*) show the particulate emission characteristics namely particle number-size distribution, number concentration of NMPs, and AMPs, and CMD of particles emitted from mineral diesel, B20 and B40 fueled engine at different SoMI timings. Results showed that advancing SoMI timing reduced the number of particles in the exhaust due to more time available for fuel–air mixing. This prevented the formation of fuel-rich zones, which was the main source of particulate nuclei formation. With advancing SoMI timing, the peak of particle number-size distribution curve shifted towards larger sized particles. This showed the formation of more agglomerates due to relatively inferior in-cylinder conditions at the time of fuel injection. In the absence of intense in-cylinder conditions, incomplete combustion produced several organic species such as polycyclic aromatic hydrocarbons (PAHs), secondary aerosols, etc., which promoted particulate agglomeration during post-combustion processes. Similar to FIP variations, SoMI variations also exhibited that biodiesel blends have inferior fuel spray characteristics compared with baseline mineral diesel. With increasing biodiesel fraction in the test fuels, the peak of number-size distribution shifted toward larger particles; however, this tendency reduced at advanced SoMI timings. Figures 7(*g*)–7(*i*) showed that AMPs emitted from the test fuels were higher compared with NMPs at all SoMI timings. With advanced SoMI timings, number concentrations of both NMPs and AMPs decreased slightly. CMD of particles emitted from all test fuels showed good agreement with the spray characteristics in the CVSC. For mineral diesel and B20, CMD of particles increased with advancing SoMI timing; however, B40 showed relatively smaller CMD of particles at very advanced SoMI timings. This trend can be also seen in number-size distribution of particles, where NMPs became more dominant comparatively. This was attributed to the combined effect of inferior fuel properties of B40 and in-cylinder conditions, which resulted in inferior fuel–air mixing, leading to formation of higher number of smaller particles.

4 Conclusions

In this study, spray characterization of mineral diesel, B20 and B40, was done in a CVSC at different FIPs (400, 700, and 1000 bars) and APs (10, 20, and 30 bars). Increasing FIP resulted in improved spray characteristics such as longer spray penetration length (L_s); however, this also led to the possibility of spray impingement on the piston lips and cylinder walls at higher FIPs. Increasing spray cone angle (θ_s) at higher APs was another important observation, which showed superior fuel atomization, leading to improved fuel–air mixing. A comparison of different test fuels showed that fuel spray characteristics of B20 were close to baseline mineral diesel. However, B40 exhibited relatively inferior fuel spray characteristics compared with baseline mineral diesel. Relatively longer L_s and smaller θ_s of B40 provided smaller surface spray area for fuel droplet-air interactions, which resulted in the formation of fuel-rich zones in the engine combustion chamber. Findings of CVSC experiments were validated by combustion and particulate emission results of the single-cylinder research engine experiments performed using the same test fuels and identical experimental conditions. Combustion results showed that fuel injection parameters such as FIP and SoMI timing should be optimized for stable combustion. In this study, intermediate FIP (700 bar) and slightly advanced SoMI timings were found to be suitable for all test fuels. Among different test fuels, B20 was found to be more suitable compared with B40 for partial replacement of mineral diesel, which is in line with the finding of spray investigations. Slightly higher particulate emissions were observed from the engine fueled with biodiesel blends, which also showed a good agreement with the findings of CVSC spray investigations. Increased biodiesel fraction in the test fuels degraded spray characteristics, which was clearly visible in the particulate characterisation results. Overall, this study presented a good correlation between the findings of fundamental spray investigations carried out in a CVSC and engine experiments performed in a state-of-the art single cylinder research engine.

References

[1] Agarwal, A. K., Gadekar, S., and Singh, A. P., 2017, "In-Cylinder Flow Evolution Using Tomographic Particle Imaging Velocimetry in an Internal Combustion Engine," ASME J. Energy Resour. Technol., **140**(1), p. 012207.

[2] Singh, A. P., and Agarwal, A. K., 2016, "Diesoline, Diesohol, and Diesosene Fuelled HCCI Engine Development," ASME J. Energy Resour. Technol., **138**(5), p. 052212.

[3] Patel, C., Hwang, J., Chandra, K., Agarwal, R. A., Bae, C., Gupta, T., and Agarwal, A. K., 2018, "In-Cylinder Spray and Combustion Investigations in a Heavy-Duty Optical Engine Fueled With Waste Cooking Oil, Jatropha, and Karanja Biodiesels," ASME J. Energy Resour. Technol., **141**(1), p. 012201.

[4] Fu, W., Li, F., Meng, K., Liu, Y., Shi, W., and Kin, W., 2019, "Experiment and Analysis of Spray Characteristics of Biodiesel Blending With Di-n-Butyl Ether in a Direct Injection Combustion Chamber," Energy, **185**, pp. 77–89.

[5] Singh, A. P., and Agarwal, A. K., 2018, "Evaluation of Fuel Injection Strategies for Biodiesel-Fueled CRDI Engine Development and Particulate Studies," ASME J. Energy Resour. Technol., **140**(10), p. 102201.

[6] Roy, M. M., 2009, "Effect of Fuel Injection Timing and Injection Pressure on Combustion and Odorous Emissions in DI Diesel Engines," ASME J. Energy Resour. Technol., **131**(3), p. 032201.

[7] Li, F., Yi, B., Fu, W., Song, L., Liu, T., Hu, H., and Lin, Q., 2019, "Experimental Study on Spray Characteristics of Long-Chain Alcohol-Diesel Fuels in a Constant Volume Chamber," J. Energy Inst., **92**(1), pp. 94–107.

[8] Mohan, B., Yang, W., Tay, K. L., and Yu, W., 2014, "Experimental Study of Spray Characteristics of Biodiesel Derived From Waste Cooking Oil," Energy Convers. Manage., **88**, pp. 622–632.

[9] Agarwal, A. K., Dhar, A., Gupta, J. G., Kim, W. I., Lee, C. S., and Park, S., 2014, "Effect of Fuel Injection Pressure and Injection Timing on Spray Characteristics

and Particulate Size–Number Distribution in a Biodiesel Fuelled Common Rail Direct Injection Diesel Engine," Appl. Energy, **130**, pp. 212–221.
[10] Agarwal, A. K., Park, S., Dhar, A., Lee, C. S., Park, S., Gupta, T., and Gupta, N. K., 2018, "Review of Experimental and Computational Studies on Spray, Combustion, Performance, and Emission Characteristics of Biodiesel Fueled Engines," ASME J. Energy Resour. Technol., **140**(12), p. 120801.
[11] Agarwal, A., Sharma, N., Singh, A. P., Kumar, V., Satsangi, D. P., and Patel, C., 2019, "Adaptation of Methanol–Dodecanol–Diesel Blend in Diesel Genset Engine," ASME J. Energy Resour. Technol., **141**(10), p. 102203.
[12] Shi, X., Pang, X., Mu, Y., He H., Shuai S., Wang J., Chen H., and Li R., 2006, "Emission Reduction Potential of Using Ethanol-Biodiesel-Diesel Fuel Blend on a Heavy-Duty Diesel Engine," Atmos Environ., **40**(14), pp. 2567–2574.
[13] Wu, Z., Zhu, Z., and Huang, Z., 2006, "An Experimental Study on the Spray Structure of Oxygenated Fuel Using Laser-Based Visualization and Particle Image Velocimetry," Fuel, **85**(10–11), pp. 1458–1464.
[14] Szybist, J. P., Boehman, A. L., Taylor, J. D., and McCormick, R. L., 2005, "Evaluation of Formulation Strategies to Eliminate the Biodiesel NOx Effect," Fuel Process. Technol., **86**(10), pp. 1109–1126.
[15] Tat, M. E., Van Gerpen, J. H., and Wang, P. S., 2004, "Fuel Property Effects on Injection Timing, Ignition Timing and Oxides of Nitrogen Emissions From Biodiesel-Fueled Engines," ASAE/CSAE Annual International Meeting, Ottawa, Ontario, Canada, Paper No. 046081.
[16] Bohl, T., Tian, G., Smallbone, A., and Roskilly, A. P., 2017, "Macroscopic Spray Characteristics of Next-Generation Bio-Derived Diesel Fuels in Comparison to Mineral Diesel," Appl. Energy, **186**, pp. 562–573.
[17] Kegl, B., and Lesnik, L., 2018, "Modeling of Macroscopic Mineral Diesel and Biodiesel Spray Characteristics," Fuel, **222**, pp. 810–820.
[18] Yu, S., Yin, B., Deng, W., Jia, H., Ye, Z., Xu, B., and Xu, H., 2018, "Experimental Study on the Diesel and Biodiesel Spray Characteristics Emerging From Equilateral Triangular Orifice Under Real Diesel Engine Operation Conditions," Fuel, **224**, pp. 357–365.
[19] Tat, M. E., and Van Gerpen, J. H., 2003, "Fuel Property Effects on Biodiesel," ASAE Annual International Meeting, Las Vegas, NV, Paper No. 036034.
[20] Sayin, C., Gumus, M., and Canakci, M., 2010, "Effect of Fuel Injection Timing on the Emissions of a Direct-Injection Diesel Engine Fueled With Canola Oil Methyl Ester-Diesel Fuel Blends," Energy Fuels, **24**(4), pp. 2675–2682.
[21] Singh, P., Chauhan, S. R., Goel, V., and Gupta, A. K., 2018, "Binary Biodiesel Blend Endurance Characteristics in a Compression Ignition Engine," ASME J. Energy Resour. Technol., **141**(3), p. 032204.
[22] Yoon, S., Park, S., Suh, H., and Lee, C. S., 2011, "Effect of Biodiesel-Ethanol Blended Fuel Spray Characteristics on the Reduction of Exhaust Emissions in a Common-Rail Diesel Engine," ASME J. Energy Resour. Technol., **132**(4), p. 042201.
[23] Zhong, W., Li, B., He, Z., Xuan, T., Lu, P., and Wang, Q., 2019, "Experimental Study on Spray and Combustion of Gasoline/Hydrogenated Catalytic Biodiesel Blends in a Constant Volume Combustion Chamber Aimed for GCI Engines," Fuel, **253**, pp. 129–138.
[24] Pachiannan, T., Zhong, W., Xuan, T., Li, B., He, Z., Wang, Q., and Yu, X., 2019, "Simultaneous Study on Spray Liquid Length, Ignition and Combustion Characteristics of Diesel and Hydrogenated Catalytic Biodiesel in a Constant Volume Combustion Chamber," Renew. Energy, **140**, pp. 761–771.
[25] Goyal, H., 2014, "Microscopic and Macroscopic Spray Characterization of Biodiesel in a Constant Volume Spray Chamber," M.Tech. Thesis, Department of Mechanical Engineering, IIT Kanpur, India.
[26] Singh, A. P., Jain, A., and Agarwal, A. K., 2017, "Fuel-Injection Strategy for PCCI Engine Fueled by Mineral Diesel and Biodiesel Blends," Energy Fuels, **31**(8), pp. 8594–8607.
[27] Jain, A., Singh, A. P., and Agarwal, A. K., 2017, "Effect of Fuel Injection Parameters on Combustion Stability and Emissions of a Mineral Diesel Fueled Partially Premixed Charge Compression Ignition (PCCI) Engine," Appl. Energy, **190**, pp. 656–669.
[28] Singh, A. P., Pal, A., and Agarwal, A. K., 2016, "Comparative Particulate Characteristics of Hydrogen, CNG, HCNG, Gasoline and Diesel Fueled Engines," Fuel, **185**, pp. 491–499.
[29] Agarwal, A. K., Singh, A. P., and Pal, A., 2017, "Effect of Laser Parameters and Compression Ratio on Particulate Emissions From a Laser Ignited Hydrogen Engine," Int. J. Hydrogen Energy, **42**(15), pp. 10622–10635.
[30] Ejim, C., Fleck, B., and Amirfazli, A., 2007, "Analytical Study for Atomization of Biodiesels and Their Blends in a Typical Injector: Surface Tension and Viscosity Effects," Fuel, **86**(10–11), pp. 1534–1544.
[31] He, C., Ge, Y., Tan, J., and Han X., 2008, "Spray Properties of Alternative Fuels: A Comparative Analysis of Biodiesel and Diesel," Int. J. Energy Res., **32**(14), pp. 1329–1338.
[32] Feng, Z., Zhan, C., Tang, C., Yang, K., and Huang, Z., 2016, "Experimental Investigation on Spray and Atomization Characteristics of Diesel/Gasoline/Ethanol Blends in High Pressure Common Rail Injection System," Energy, **112**, pp. 549–561.
[33] Guan, L., Tang, C., Yang, K., Mo, J., and Huang, Z., 2015, "Effect of Di-NButyl Ether Blending With Soybean-Biodiesel on Spray and Atomization Characteristics in a Common-Rail Fuel Injection System," Fuel, **140**, pp. 116–125.
[34] Yuan, W., Hansen, A. C., and Zhang, Q., 2009, "Predicting the Temperature Dependent Viscosity of Biodiesel Fuels," Fuel, **88**(6), pp. 1120–1126.
[35] Ryu, J., Kim, H., and Lee, K., 2005, "A Study on the Spray Structure and Evaporation Characteristic of Common Rail Type High Pressure Injector in Homogeneous Charge Compression Ignition Engine," Fuel, **84**(18), pp. 2341–2350.
[36] Agarwal, A. K., Singh, A. P., Gupta, T., Agarwal, R. A., Sharma, N., Rajput, P., Pandey, S. K., and Ateq, B., 2018, "Mutagenicity and Cytotoxicity of Particulate Matter Emitted From Biodiesel-Fueled Engines," Environ. Sci. Technol., **52**(24), pp. 14496–14507.
[37] Agarwal, A. K., Ateeq, B., Gupta, T., Singh, A. P., Pandey, S. K., Sharma, N., Agarwal, R. A., Gupta, N. K., Sharma, H., Jain, A., and Shukla, P. C., 2018, "Toxicity and Mutagenicity of Exhaust From Compressed Natural Gas: Could This be a Clean Solution for Megacities With Mixed-Traffic Conditions?" Environ. Pollut., **239**, pp. 499–511.
[38] Askari, O., Metghalchi, H., Kazemzadeh Hannani, S., Moghaddas, A., Ebrahimi, R., and Hemmati, H., 2012, "Fundamental Study of Spray and Partially Premixed Combustion of Methane/Air Mixture," ASME J. Energy Resour. Technol., **135**(2), p. 021001.
[39] Askari, O., Metghalchi, H., Kazemzadeh Hannani, S., Hemmati, H., and Ebrahimi, R., 2014, "Lean Partially Premixed Combustion Investigation of Methane Direct-Injection Under Different Characteristic Parameters," ASME J. Energy Resour. Technol., **136**(2), p. 022202.